PHILOSOPHICAL TRANSACTIONS A

Research

CrossMark
click for updates

Author for correspondence:
J. Burguete
e-mail: javier@unav.es

Experimental dynamics in magnetic field-driven flows compared to thermoconvective convection

I. Cortés-Domínguez, J. Burguete and H. L. Mancini

Departamento de Física y Matemática Aplicada, Universidad de Navarra, Irunlarrea 1, 31008 Pamplona, Spain

We compare the dynamics obtained in two intermediate aspect ratio (diameter over height) experiments. These systems have rotational symmetry and consist of fluid layers that are destabilized using two different methods. The first one is a classical Bénard–Marangoni experiment, where the destabilizing forces, buoyancy and surface tension, are created by temperature gradients. The second system consists of a large drop of liquid metal destabilized using oscillating magnetic fields. In this configuration, the instability is generated by a radial Lorentz force acting on the conducting fluid. Although there are many important differences between the two configurations, the dynamics are quite similar: the patterns break the rotational symmetry, and different azimuthal and radial wavenumbers appear depending on the experimental control parameters. These patterns in most cases are stationary, but for some parameters they exhibit different dynamical behaviours: rotations, transitions between different solutions or cyclic connections between different patterns.

1. Introduction

Pattern formation in fluids has been an active field of experimental and theoretical research for more than three decades [1]. Many experiments have been performed, mainly in systems driven by thermo-convective forces, where the existence of self-organized patterns has been well known for more than a century.

Time-dependent convective patterns with very complex dynamics have been used in recent decades to perform key experiments that have become a benchmark of proofs to validate new theoretical ideas in nonlinear

THE ROYAL SOCIETY PUBLISHING

2

rsta.royalsocietypublishing.org *Phil. Trans. R. Soc. A* **373**: 20150113

dynamics, where very complex dynamical behaviours have been predicted, like chaotic dynamics in complex systems, patterns with spatio-temporal chaos [2] or control and synchronization of complex chaotic systems [3].

Many experimental results initially obtained in the framework of hydrodynamics have been reproduced in other systems with very different physical instability mechanisms and driving forces (e.g. Taylor–Couette flow, lasers, nonlinear optical systems, chemical oscillating reactions). In many experiments, the influence of the physical properties of the system, i.e. shapes, sizes, symmetries as well as other relevant parameters that have been observed, allow us now to construct more accurate mathematical models to describe the dynamics observed and to remark upon many common features between the different systems, one of the most relevant being the presence of symmetries. Thermoconvection in layers of confined fluids is probably the paradigm in this kind of experiment. There are two different families of experiments depending on whether the buoyancy force acts alone or combined with surface-tension driving forces [4], as we consider here. In both, the results are usually classified into three main regions as a function of the ratio between the horizontal characteristic dimension and the depth of the fluid layer: small, intermediate and large 'aspect ratio' Γ.

The aspect ratio Γ in thermoconvective systems is usually defined as the ratio between the horizontal dimension (i.e. in cylindrical symmetry O(2), the diameter D) and the depth of fluid d ($\Gamma = D/d$). It is clear that, for small values of the aspect ratio ($D \sim d$), the lateral boundary conditions and symmetries will influence the selection of the pattern and the dynamics obtained. On the other hand ($D \gg d$, large aspect ratio), these boundaries will scarcely be noticeable. If the ratio is smaller than the horizontal correlation length λ (non-dimensional) for the variables of the system, a coherent system is obtained, where a phase could be defined for any point of the system. For larger dimensional systems, different parts separated by a distance greater than λ can act as independent subsystems with different dynamics. When the system is heated from below sufficiently, the fluid becomes convective, and near threshold a cellular stationary structure is the asymptotic final state, exhibiting the influence of symmetry. In extended homogeneous layers of high Prandtl number fluids, the final pattern is always stationary. Nevertheless, when the system is confined in one of the transverse spatial dimensions, the pattern can drift [5] or waves may appear in both pure Bénard–Marangoni systems [6,7] or laterally heated layers [8,9].

We will focus here on cylindrically symmetric layers (O(2)) confined in containers homogeneously heated from below. For small aspect ratios, the patterns that normally appear have been classified in [10,11] as a function of the analytical solutions and have been later verified experimentally in [12–14]. Patterns have been classified into *modes* by the two indices (m, n) based on the analytical solution proposed by Rosenblat *et al*. [10,11] which are observed in an experiment as an ordering for the patterns based on two numbers reflecting the number of radial (n) and azimuthal (m) partitions in the planform. We will keep this definition here. In the intermediate aspect ratio (IAR) region, both experiments and theoretical works are relatively scarce. The asymptotic stationary patterns near threshold have been studied in [15–17]. The upper view of the patterns obtained near threshold consist of a single central polygonal cell with five to eight sides, with an inscribed diameter near the solution corresponding to $n = 1$, completed by external half-cells corresponding to radial partitions with $m = 5$–8, as shown in figure 1. Up to the maximum diameter of the container scaled, we never obtained $m = 4$ or $m > 8$.

Dynamic behaviours in IAR patterns appear when the driving force is increased and maintained fixed not too far from threshold (distance from threshold is defined by the supercriticality: $\epsilon = (T - T_c)/T_c$). In this kind of system, to define threshold, two non-dimensional numbers (and their ratio) are necessary: the Rayleigh number for the influence of buoyancy and the Marangoni number for surface tension [18].

We now remark on two movements appearing in IAR convection near threshold. The first dynamical situation is the rotation of all the structure of convective cells as a whole. Rotations in convective patterns with O(2) symmetry were predicted in [19] and observed for small aspect ratio (SAR) systems in [12–14,20]. In IAR systems, this situation was studied in [15], where central
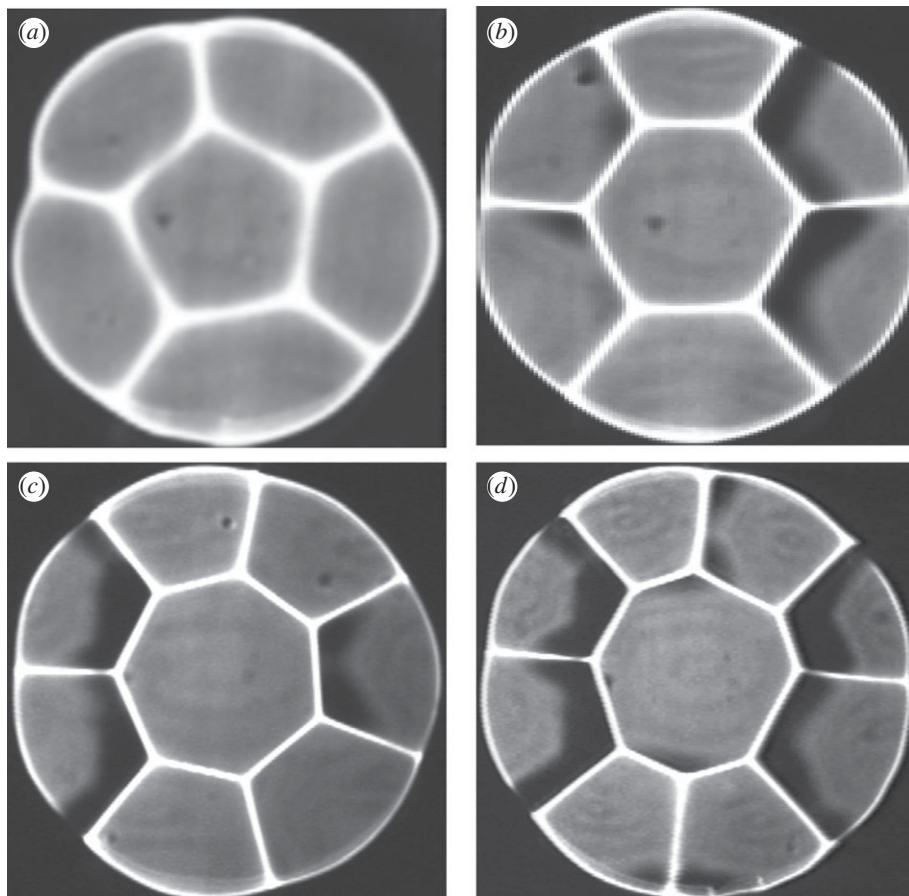
Figure 1. Shadowgraphs of the four structures appearing: (*a*) $n = 1$ and $m = 5$, $\Gamma = 9.6$, $\Delta T = 7.6$ K; (*b*), (*c*) and (*d*) with $n = 1$ and $m = 6, 7$ and 8, $\Gamma = 10.2$, $\Delta T = 10.2, 10.8$ and 12.3 K (silicone oil 350 cSt).

polygonal cells with different m rotate as a whole. The second dynamical situation is the transition between patterns with different azimuthal number m from m to $(m + 1)$ or $(m - 1)$.

In this work, the former dynamical situation will be compared with the dynamics appearing in a very different system, a layer of conductive fluid driven by an external magnetic field. When this field becomes time-dependent, it can generate a destabilizing force that produces surface waves or other instabilities [21–23].

There are a few experimental works related to the study of instabilities in fluids under the action of external magnetic fields [24–26]. This effect depends on two sets of parameters: the fluid layer properties (electrical conductivity, layer depth, diameter) and the magnetic field characteristics (frequency and intensity). When the magnetic field frequencies are large, the instabilities grow due to forces localized near the surface. On the other hand, for low frequency ranges, those forces may penetrate and produce bulk forces. Many experimental works have been developed for the large frequency regime, but there is a lack of results in the domain of low frequencies because of its limited potential applications. We shall study the low range of frequencies (0.1–10 Hz).

Following the previous work of Burguete *et al.* [27], we will focus on a configuration where a thin axisymmetric conducting fluid layer with a free surface is forced through a time-dependent magnetic field parallel to the axis of a circular cell. In Burguete's work, the magnetic field always had the same orientation: the magnetic field was $B_0 + B_1 \sin(\omega_B t)$, with $B_1 < B_0$. In this paper, we present results obtained with either zero (oscillation between both possible orientations in a cycle)

or non-zero mean magnetic field. This field generates in the fluid azimuthal currents that interact again with the magnetic field, producing a radial force (Lorentz force). Owing to the nature of the external magnetic field applied, the oscillatory component of the Lorentz force will have a frequency twice ω_B. Any perturbation that deviates the system from axisymmetry can produce an azimuthal force that destabilizes the fluid and a flow can be created.

This work is organized as follows. After this introduction, the experimental set-ups for both systems are described in §2. Section 3 is devoted to presenting the results obtained in both systems, followed by a discussion comparing the systems and the conclusion in §4.

2. Experimental set-ups

Although the instabilities that produce the patterns have a very different origin, the experimental set-ups where these processes have been analysed share many features. Their description has been divided into three different parts: the experimental cells, where we describe each one of the containers; the optical set-up, where we describe how the observations were made; and the data processing, where we present the different ways in which we have processed the data.

(a) Experimental cells

(i) Thermoconvective experiment

The experimental thermoconvective set-up used in IAR experiments is very similar to others described in previous works of our group on small (SAR) and large (LAR) aspect ratios. The O(2) symmetry is imposed onto the fluid layer by a cylindrical container. Figure 2*a* presents a cross section of the container with the real dimensions used and displays the different parts: (1) the insulating external walls with a top cover on the upper part, (2) a copper disc that conducts the heat from an electrical heater to the bottom surface of the fluid layer, (3) Plexiglas sidewall in contact with the fluid layer to define the aspect ratio value, (4) Plexiglas washer to define an upper region open to air and (5) the electrical heater (in black).

We used high Prandtl number fluids (silicone oils of 100–350 cSt) in order to have a clear distinction between the regions of two-dimensional, three-dimensional and time-dependent convections [18].

(ii) Magnetohydrodynamic experiment

The main geometry of the set-up is a Teflon cylindrical cavity (diameter of 84 mm), where we placed a large drop of eutectic InGaSn alloy. This drop, although with an IAR ($D \gg d$), is small compared with the inner diameter of the container. So, to retain the drop centred in the cell and in the external applied magnetic field, a small depression was milled in the centre of the bottom part (depression diameter of 40 mm), as can be observed in figure 2*b*. The fluid adopts the form of a thick circularly shaped fluid layer and remains centred (figure 2). The InGaSn drop is up to 20 mm depth.

We use this alloy because of its electrical conductivity and, furthermore, the InGaSn alloy remains liquid at room temperature. Like any other electrically conducting fluid, it will react to the action of external magnetic fields. The surface of this large drop acts as a mirror, and the fluid itself is opaque. We have no access to the inner part of this drop, only to the surface deformations. An upper layer of HCl has been used to prevent oxidation of the eutectic alloy. It is important to note that, apart from the electrical conductivity, this fluid has no special magnetic properties (i.e. as in ferrofluids or any other fluid family with specific magnetic properties).

Once the fluid is chosen, the only parameter that can be modified is the geometry: the layer depth and diameter. Nevertheless, as these two parameters are closely related (the shape of the droplet is free, there are no external restrictions), we use as parameter the volume of liquid metal.

The destabilization of the droplet can be achieved using external electrical currents and/or magnetic fields. In our experimental set-up, we force the system with external magnetic
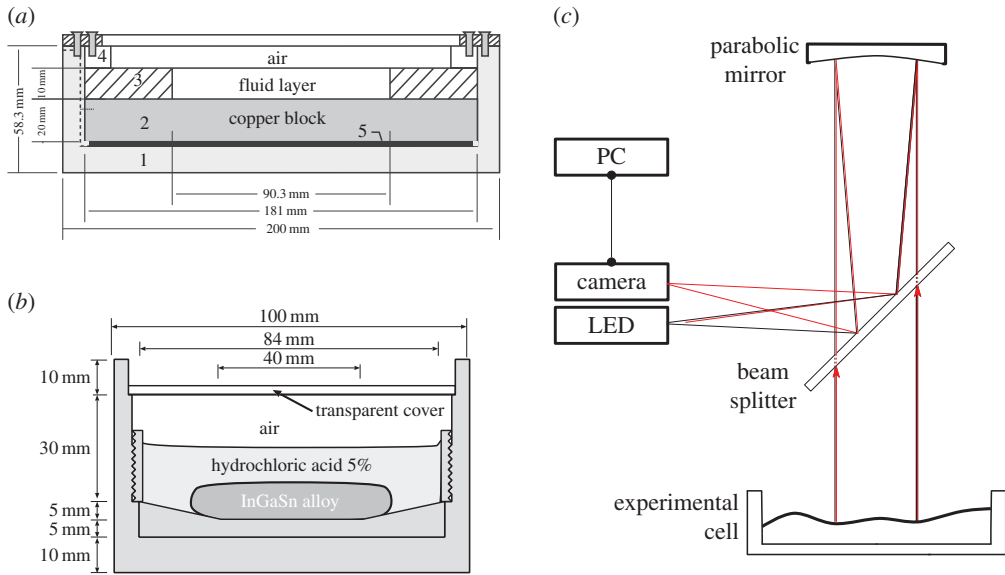
Figure 2. Cross sections of the experimental cells used. (*a*) Thermoconvective experiments: outline of the fluid container showing (1) insulating cell, (2) copper disc, (3) Plexiglas sidewall, (4) Plexiglas washer and (5) electrical heater. (*b*) Magnetohydrodynamics (MHD) experiments: a large drop of a liquid metal (InGaSn alloy) immersed in a hydrochloric acid bath to prevent oxidation. (*c*) Sketch of the observation system used in both experiments. (Online version in colour.)

fields without external currents. Instead, we introduced time-dependent magnetic fields. These magnetic fields are oriented in the axial direction (parallel to gravity) and are homogeneous (better than 1%) in the fluid layer. This magnetic field has a sinusoidal evolution, and so it is fully determined by the frequency ω_B:

$$\boldsymbol{B}(t) = [B_0 + B_1 \sin(\omega_B t)]\, \hat{\boldsymbol{k}}.$$

When $B_0 = 0$, the applied magnetic field has zero mean, and thus it oscillates between two different orientations $\pm B_1 \hat{\boldsymbol{k}}$. On the other hand, when $B_0 > B_1$, the magnetic field has an average value of B_0 and preserves the orientation determined by $B_0 \hat{\boldsymbol{k}}$.

These time-dependent magnetic fields produce in the fluid layer azimuthal induced currents. These currents interact again with the magnetic field, producing radial Lorentz forces. So, the second group of parameters that we need to set are the magnetic field properties. Depending on the intensity (B_0 and B_1) and frequency of the magnetic field and on the dimensions of the liquid droplet, we can define two independent non-dimensional parameters: the interaction parameter and the Reynolds number.

The interaction parameter measures how important the Lorentz force is compared with inertia, $N = B_i^2 \sigma / \rho \omega_B$; here σ and ρ are the electrical conductivity and density of the fluid, B_i and ω_B are the intensity and frequency of the magnetic field. The definition of the Reynolds number is the classical one and relates inertia to viscous forces, $Re = \omega_B L^2 / \nu$, with ν the kinematic viscosity of the fluid. A third parameter, the Hartmann number, can be derived from these two and used to express the ratio between viscous and Lorentz forces, $Ha = B_i L \sqrt{\sigma / \nu \rho}$.

These magnetic fields are generated by coils placed around the experimental cell, so the axis of the cell (and consequently the droplet axis) is aligned with the centre of the coil. The current is modulated with a frequency variator (allows us to control the frequency and intensity). The magnetic field generated will be proportional to the modulated current. It is possible to modify the current frequency in the range of very low frequencies $f_B \in [0.1–10]$ Hz. These frequencies are small enough to ensure that the magnetic field penetrates the whole fluid layer. For this fluid, frequencies higher than 100 Hz are not able to penetrate the surface (skin effect) and so only

6

rsta.royalsocietypublishing.org *Phil. Trans. R. Soc. A* **373**: 20150113

surface forces will be produced. The power supply that controls the system allows us to reach intensities of 60 A, giving rise to magnetic field intensities up to 70 mT.

(b) Optical system

The optical system is based on the method developed by Foucault [28]. When a beam of parallel light arrives perpendicular to a fluid layer, it is reflected (partially if this is a transparent fluid like silicone oil, completely if a liquid metal) backwards if the surface if flat. Any surface deviation of the fluid will modify the orientation of the reflected light. Only areas where the fluid remains perpendicular to the incident beam will return the light like a mirror. This can be used to determine very precisely the flatness or curvature of an unstable fluid layer (figure 2c). This can be obtained with an optical set-up reminiscent of a telescope: placing an LED at the focal point of a parabolic mirror, which redirects the light along the axis of the cylindrical cell. Using a beam splitter, the light beam arrives perpendicular to the free surface of the fluid. Introducing a slight aberration on the telescope, the final image will appear slightly displaced from the point source: a camera can be located in that position, so we will recover bright lines when the surface is flat, and different grey levels depending on the curvature (figure 2c).

In both set-ups, before the instabilities that produce the patterns, the fluid layer remains flat and a bright disc is observed on the screen. Any instability produces small surface deviations of the fluid surface. The set-up allows us to record the top view to study the deflections of the surface. Any deflection will appear in the camera as bright regions (beam of light perpendicular to this area) or dark regions (areas in which the reflected focus has been displaced as a result of surface modulation). We can study the dynamical behaviour of the system as a result of the grey scale between the bright and dark regions that appears with the modulations. In the particular case of the thermoconvective experiment, the bright lines localize the cold regions where the fluid in convection is going downwards and the surface curvature is plane, maximizing the light reflected back.

There are slight differences between each one of the optical set-ups. The thermoconvective dynamics is very slow compared with the magnetohydrodynamic (MHD) experiment. In the first case, the camera is connected to a computer that allows us to record extremely slow dynamics: each one of the frames is recorded with a sampling period that can be of some minutes. On the other hand, the MHD experiments deal with excitation frequencies up to 10 Hz, so we must record the dynamical behaviour with sampling frequencies higher than 20 Hz. When this was not possible, we have used techniques using two sampling frequencies that allows us to extend the acquisition range up to 100 Hz. All these images are digitally recorded for further processing.

(c) Data processing

The results that we report in this work concern dynamics in the azimuthal direction. To accurately determine these displacements, a specific procedure was created. From the top view obtained with the optical system described in the previous section, we determine the position of the axis of symmetry. Then, we select a radius R that determines a circumference whose azimuthal dynamics is being analysed: the intensities of the pixels along the perimeter of this circle are recorded (yellow dashed lines in figure 3a–c). This circumference is then unfolded on an image over a straight line. This procedure is repeated with a fixed sampling frequency large enough to recover the dynamics, and each one of the lines is stacked below the others. We obtain what is known as a spatio-temporal diagram, where the time variable is recorded in the vertical direction, and the azimuthal behaviour in the horizontal directions as shown in figure 3d.

When the pattern is stationary, the bright lines are vertical along the time. When the pattern is moving, displacements are registered by controlling the positions of the bright lines, as can be observed in figure 3. Special care has to be taken when dealing with the MHD experiments. In this case, the forcing mechanism already has its own frequency f_B, and this can contaminate the observed dynamics. So, instead of presenting the whole spatio-temporal diagram, which presents
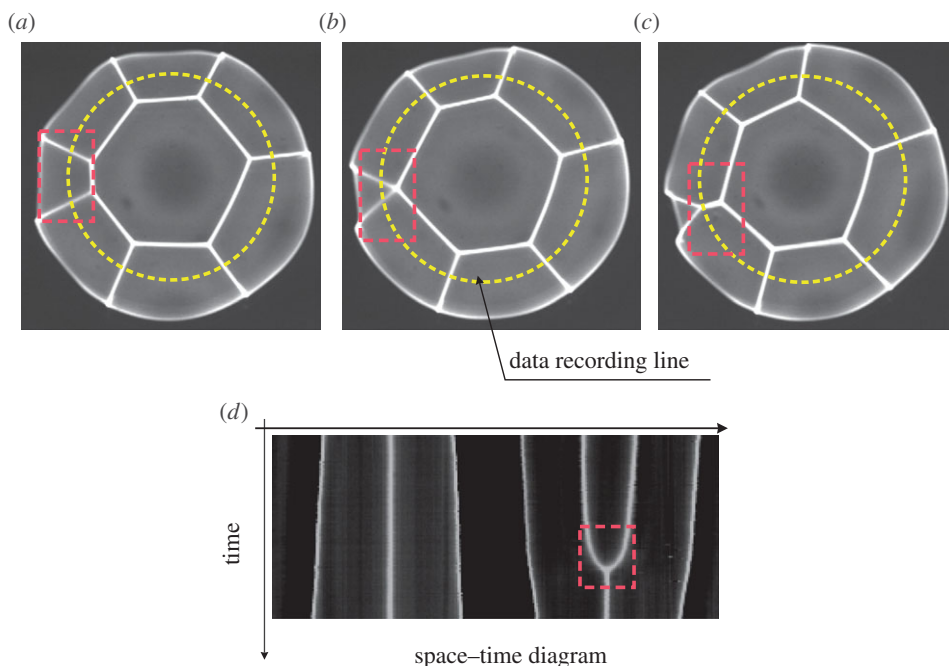
Figure 3. Bifurcation between a pattern with $n = 1$, $m = 7$ to another with $n = 1$, $m = 6$. (a–c) Three snapshots of the pattern. (d) Spatio-temporal diagram for the same time interval. The (red) dashed rectangles mark the regions where the transition takes place. (Online version in colour.)

the whole set of frequencies of the problem, we present only a set of frequencies, as if we had used a digital stroboscope.

3. Results and discussion

Although both systems rely on instabilities that appear in axisymmetric fluid layers, this is the only common feature. In the thermoconvective experiment, the destabilizing forces have two origins: a bulk force (buoyancy) in the vertical direction and a surface force (surface tension-driven) in the horizontal direction. Even more, the driving parameter, the temperature gradient, is a scalar magnitude that remains constant in time. In the MHD problem, there is only one destabilizing force, the Lorentz force. In this latter case, the force operates in the radial direction, reversing its orientation with a frequency that depends on the forcing frequency ω_B. The driving parameter, the magnetic field, is a vectorial magnitude with a sinusoidal modulation. These differences point *a priori* to different dynamical regimes, but what we have found are instead similar behaviours with many shared characteristics.

(a) Thermoconvection

There are no previous experimental or theoretical works reporting dynamical results in IAR. Static observations of one central hexagonal cell have been reported by Cerissier *et al.* [29], who observed that, inducing hexagonal cells from three different initial aspect ratios, relaxation brings the system to the same final imposed state. Depending on supercriticality, a hexagonal cell has been observed for aspect ratios $\Gamma = 9.33$ in [30]. The other structures appearing in figure 1, with one polygonal cell centred in a cylindrical container, have been reported in [13] and systematically studied in [15]. (For the values used in this work, see the captions in the figures.)
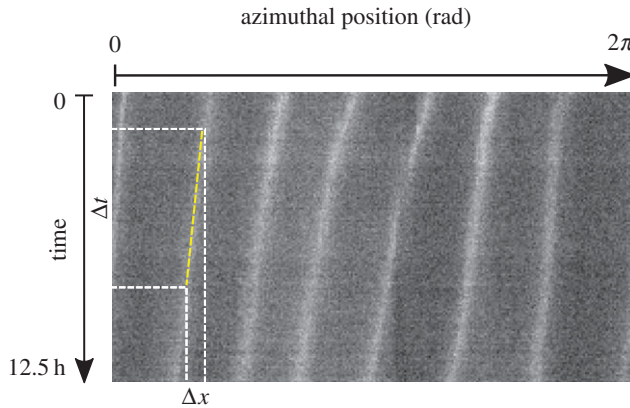
Figure 4. Rotation of a heptagon as a whole ($\epsilon = 0.7$, rotation velocity is about $2°\,h^{-1}$). (Online version in colour.)

Scanning with a frequency higher than the natural times of the pattern observed, we can have a sampled pattern in real time. In the figures, the image shows that the central pattern is changing from a heptagon to a hexagon by the absorption of one convective cell for the laterals that are increasing their size, reducing the total number of radial partitions from $m = 7$ to 6 (in this work, the intensity was recorded every 3–5 min). The bifurcation in the time–space diagram appears when the two lateral bright lines (regions where fluid is going down) of the cell that is being eliminated collapse into one, measured at a distance D from the centre. Similar behaviours have been observed in Rayleigh–Bénard problems, when a wavenumber is selected that lies outside the stability range. The system spontaneously modifies the wavelength through an Eckhaus instability [31]. In our problem, however, both patterns, the original and the new, are stable.

When the dynamics is a pure rotation of the pattern as a whole, the space–time diagram appears as in figure 4 with all the bright lines having approximately the same angle. The tangential group velocity at the circumference of diameter D (which can be selected) can be measured from the values of $\Delta x/\Delta t$ in the diagram. The width of the pattern is a turn, i.e. $360° = 2\pi R$, and in figure 4, the heptagon rotates anticlockwise with an angular velocity of approximately $2°$ per hour $\omega_B(D \sim d) = 2°\,h^{-1}$.

(b) Magnetohydrodynamics

In the MHD experiments, we must be careful what we call a dynamical pattern. Because of the time-dependent nature of the forcing mechanism, there are no stationary patterns, in the sense that the observed pattern is always the same, no matter when the measurement is done. The Lorentz force alternates its radial orientation in a forcing cycle, pointing outwards or towards the centre of the container. This is because we must combine the magnetic field (whose orientation can change) and the azimuthal current, whose direction depends on the temporal evolution of the magnetic field (i.e. increasing or decreasing). So we must differentiate between the dynamics induced by the forcing, and that of the pattern itself. As described above, this has been determined by recording the pattern position only at specific phase positions (specific moments) of the forcing cycle. This approach is equivalent to a digital stroboscope. In this way, we can compare the pattern position in different forcing cycles.

As described above, there are three parameters in this experiment: the volume of the liquid droplet, and the frequency and intensity of the magnetic field. For a fixed volume, we have recorded the different patterns that may appear. This phase space can be divided into two different regions, the first one where the droplet does not break any of the symmetries, and so an axisymmetric oscillating surface is observed, and a second region where the droplet spontaneously breaks the azimuthal symmetry (for small volumes) and radial modes have been
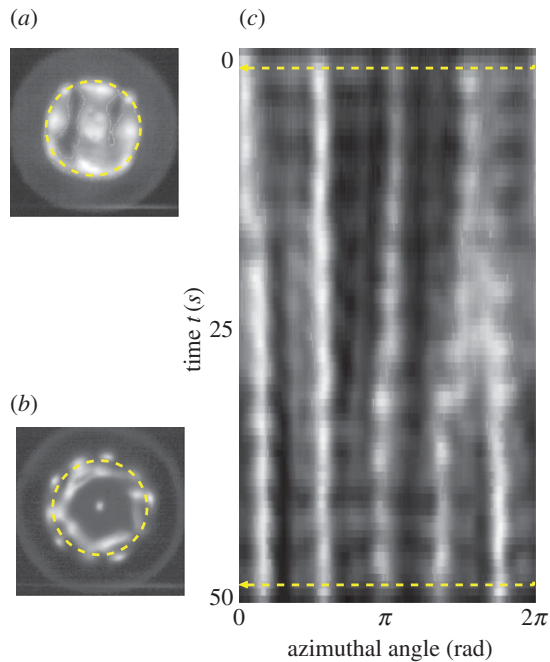
Figure 5. Transition between two different patterns in MHD experiments. The forcing frequency is $f_B = \omega_B/2\pi = 3.06$ Hz, $B_0 = 54$ mT and $B_1 = 10$ mT. On the left, initial (*a*) and final (*b*) snapshots of the observed pattern. (*c*) Spatio-temporal diagram recovered tracking the images. The (yellow) dashed lines mark the correspondence between the circumferences marked on (*a*,*b*) and their position on the spatio-temporal diagram (*c*). (Online version in colour.)

observed (for large drops). These regions where the symmetry breaking is observed correspond to narrow regions around resonant frequencies. For these frequencies, the larger the magnetic field, the larger the amplitude of the patterns. We have also observed patterns with different symmetries that can be reached for the same parameter values (coexistence). A more detailed explanation can be found in [27,32]. The observed patterns may have any azimuthal wavenumber between $m = 3$ and $m = 10$. Although there are some indications that an $m = 2$ pattern is possible, it is very difficult to separate this mode from other sources of experimental noise.

In these experiments, we have observed connections between solutions with different symmetries. These connections can be a slow connection between two solutions when both are possible (this system is characterized for being multistable, i.e. multiple patterns can be found for the same experimental parameters) or fast heteroclinic orbits between two patterns with different symmetry in a single cycle. Up to now, we have not detected the drift of the pattern as a whole with constant velocity as has been observed in the thermoconvective experiment (figure 4). Nevertheless, we have observed a drift with a velocity that fluctuates. We believe that this drift is produced by small random fluctuations: the dynamics can be assimilated to a one-dimensional 'drunk man walk' problem giving rise to a fluctuating drift with a very large characteristic time. Further work is under progress to confirm this statement.

In thermoconvective experiments, large values of the temperature gradient produce spatio-temporal disorder. A similar behaviour has been observed in MHD for large values of the driving force (large magnetic fields) in other experiments [24–26]. This regime cannot be reached in our set-up, as it is optimized for small values of the interaction parameter.

The first dynamical behaviour, the transition between two solutions, is very similar to the case of the thermoconvective experiment. With a very slow dynamics (compared with other times of the forcing mechanisms), a transition is observed between the solutions $m = 4$ and $m = 5$ (figure 5). This behaviour has been observed when a mean field is present ($B_0 > B_1$) and has not been
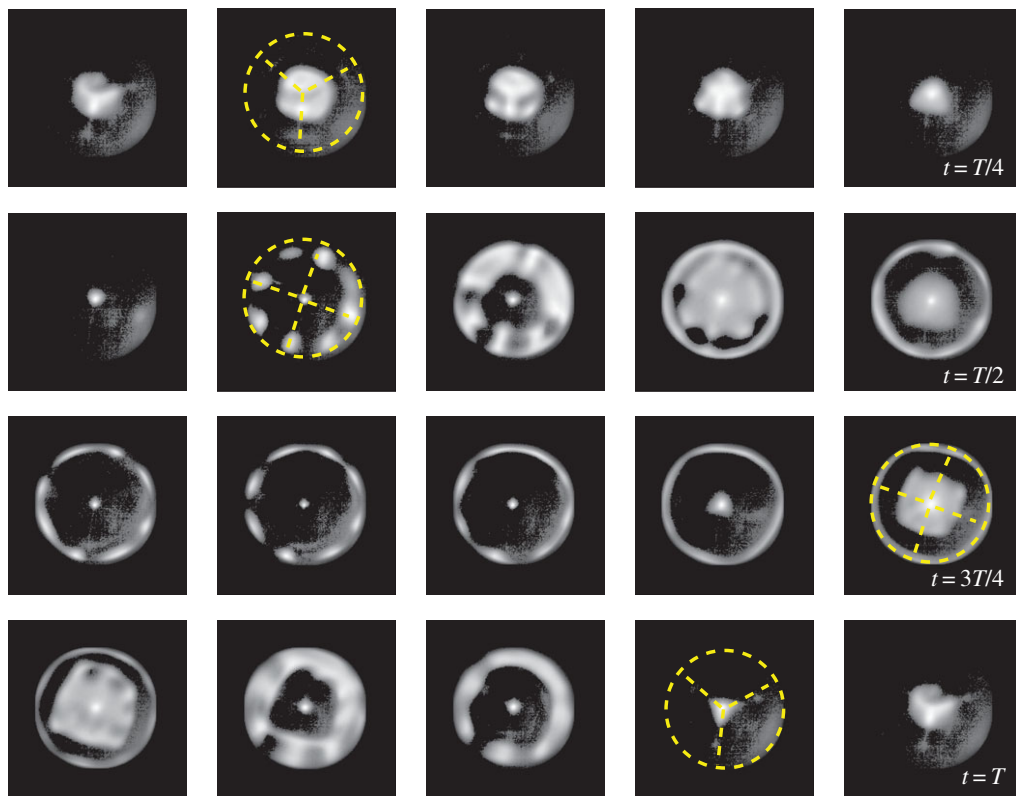
Figure 6. Snapshots of an orbit of the heteroclinic cycle: the cycle starts at the top left $t = 0$, and increases from left to right, and then from top to bottom, until the cycle closes at $t = T$ at the bottom right. This period corresponds to one half of the forcing period $2\pi / \omega_B$. Experimental parameters: $f_B = \omega_B/2\pi = 2.1$ Hz, $B_0 = 0$, $B_1 = 42$ mT. (Online version in colour.)

observed when the mean magnetic field is zero, $B_0 = 0$. The reason for this difference could be that the magnetic field in the second set of experiments (with $B_0 = 0$) is much more homogeneous in space and has a nearly perfect harmonic behaviour in time compared with the non-zero average magnetic field, $B_0 \neq 0$, experiments. In this last case, these deviations from the ideal B will induce fluctuations of the Lorentz force, and so the system can cross the barrier between the different solutions available, as in a noise-activated problem.

On the other hand, for both configurations of the magnetic field, we have observed a very fast dynamics that corresponds to a heteroclinic orbit between two different solutions with different symmetries. An example of this dynamics is presented in figure 6. This figure presents one half of the forcing period (because of the shape of the Lorentz force, $j \times B$, this term oscillates with a frequency that is twice the forcing frequency). In the case presented here, there is a fast transition between an $m = 3$ pattern and an $m = 4$ pattern. Other configurations where $m = 5$ and 7 have also been observed.

All these dynamics correspond to cycles with different azimuthal wavenumbers but with the same radial wavenumber. For higher values of the radial wavenumber, other patterns have been observed, but up to now we have not been able to detect clear dynamical behaviours.

4. Conclusion

We have presented results for two different experimental set-ups. Both systems have rotational symmetry and analyse the behaviour of a fluid layer with a free surface. Nevertheless, the physical mechanisms that trigger the instabilities are very different: in the thermoconvective experiment, bulk and surface forces driven by the vertical temperature gradient; in the MHD

11

rsta.royalsocietypublishing.org *Phil. Trans. R. Soc. A* **373**: 20150113

experiment, oscillating radial Lorentz forces produced by time-dependent magnetic fields. Despite these very important differences, the observed dynamics are similar.

In the thermoconvective case, we have observed static patterns that break the azimuthal symmetry. But for some experimental parameters, these patterns can (i) rotate with a nearly constant velocity or (ii) transit to a different azimuthal wavenumber m. For the studied parameters, this last transition is always from a given wavenumber m to $m + 1$ or $m - 1$. Other dynamical behaviours have been observed for higher supercriticality, but they were not included because of their complexity.

In the MHD experiment, similar behaviours were obtained. Static patterns breaking the rotational symmetry with $m \in [3\text{--}10]$ were observed. Different dynamics were observed: (i) the patterns can drift, although in this case the velocity is not constant, but it fluctuates; and (ii) we have found alternation between patterns. In this latter case, we can differentiate between two regimes. The first one corresponds to the observed behaviour in thermoconvection, a transition from m to $m \pm 1$, similar to Eckhaus instabilities. The second one corresponds to a fast connection between the available solutions of the problem. We have presented a case with alternation between $m = 3$ and $m = 4$, but other cases with other wavenumbers (such as $m = 5$ and $m = 7$) have been observed.

References

1. Cross MC, Hohenberg PC. 1993 Pattern formation outside of equilibrium. *Rev. Mod. Phys.* **65**, 851–1112. (doi:10.1103/RevModPhys.65.851)
2. Mancini HL. 2007 Preface: New trends, dynamics and scales in pattern formation. *Eur. Phys. J. Spec. Top.* **146**, V–VII. (doi:10.1140/epjst/e2007-00163-2)
3. Boccaletti S, Grebogi C, Lai Y, Mancini H, Maza D. 2000 The control of chaos: theory and applications. *Phys. Rep.* **329**, 103–197. (doi:10.1016/S0370-1573(99)00096-4)
4. Colinet P, Legros JC, Velarde MG. 2001 *Nonlinear dynamics of surface-tension driven instabilities*. Berlin, Germany: Wiley-VCH.
5. Burguete J, Mancini HL, Perez-Garcia C. 1993 Dynamics of a secondary instability in Bénard–Marangoni convection with unidimensional heating. *Europhys. Lett.* **23**, 401–407. (doi:10.1209/0295-5075/23/6/004)
6. Burguete J, Maza D, Mancini HL. 2003 One-dimensional dynamics in locally heated liquid layers. *Physica D–Nonlin. Phenom.* **174**, 56–70. (doi:10.1016/S0167-2789(02)00682-6)
7. Burguete J, Mancini H. 2014 Localized structures in convective experiments. *Eur. Phys. J. Spec. Top.* **223**, 9–20. (doi:10.1140/epjst/e2014-02081-6)
8. Burguete J, Mukolobwiez N, Daviaud F, Garnier N, Chiffaudel A. 2001 Buoyant-thermocapillary instabilities in extended liquid layers subjected to a horizontal temperature gradient. *Phys. Fluids* **13**, 2773–2787. (doi:10.1063/1.1398536)
9. Burguete J, Chaté H, Daviaud F, Mukolobwiez N. 1999 Bekki–Nozaki amplitude holes in hydrothermal nonlinear waves. *Phys. Rev. Lett.* **82**, 3252–3255. (doi:10.1103/PhysRevLett.82.3252)
10. Rosenblat S, Davis S, Homsy G. 1982 Nonlinear Marangoni convection in bounded layers. Part 1. Circular cylindrical containers. *J. Fluid Mech.* **120**, 91–122. (doi:10.1017/S0022112082002687)
11. Rosenblat S, Homsy G, Davis S. 1982 Nonlinear Marangoni convection in bounded layers. Part 2. Rectangular cylindrical containers. *J. Fluid Mech.* **120**, 123–138. (doi:10.1017/S0022112082002699)

12. Koschmieder EL. 1993 *Benard cells and Taylor vortices*. Cambridge, UK: Cambridge University Press.

13. Ondarcuhu T, Millán-Rodríguez J, Mancini H, Garcimartin A, Pérez-García C. 1993 Bénard–Marangoni convective patterns in small cylindrical layers. *Phys. Rev. E* **48**, 1051–1057. (doi:10.1103/PhysRevE.48.1051)

14. Ramón ML, Maza D, Mancini HL. 1999 Patterns in small aspect ratio Benard–Marangoni convection. *Phys. Rev. E* **60**, 4193–4198. (doi:10.1103/PhysRevE.60.4193)

15. Ramón ML. 2000 Estudio experimental sobre formación y dinámica de estructuras espaciales en sistemas confinados. Thesis (in Spanish), University of Navarra. See http://www.unav.edu/departamento/fisica/tesis-doctorales.

16. Ramón ML, Maza D, Mancini HL, Mancho AM, Herrero H. 2001 Hexagonal structure in intermediate aspect ratio Benard–Marangoni convection. *Int. J. Bifurcation Chaos* **11**, 2279–2787. (doi:10.1142/S0218127401003899)

17. Mancini H, Maza D, Ramón ML. Benard–Marangoni convection: dynamics at intermediate aspect ratio with symmetry O(2) (unpublished, preprint available from hmancini@unav.es).

18. Mancini H, Maza D. 1997 Benard–Marangoni thermal oscillators: an experimental study. *Phys. Rev. E* **55**, 2757–2768. (doi:10.1103/PhysRevE.55.2757)

19. Crawford JD, Knobloch E. 1991 Symmetry and symmetry-breaking bifurcations in fluid dynamics. *Annu. Rev. Fluid Mech.* **23**, 341–387. (doi:10.1146/annurev.fl.23.010191.002013)

20. Maza D, Echebarria B, Perez Garcia C, Mancini H. 1996 Benard–Marangoni convection in small aspect ratio containers. *Physica Scripta* **T67**, 82–85. (doi:10.1088/0031-8949/1996/T67/016)

21. Moreau R. 1990 *Magnetohydrodynamics*. Dordrecht, The Netherlands: Kluwer.

22. Moffatt K. 1978 *Magnetic field generation in electrically conducting fluids*. Cambridge, UK: Cambridge University Press.

23. Molokov S, Moreau R, Moffatt HK (eds). 2007 *Magnetohydrodynamics, historical evolution and trends*. Dordrecht, The Netherlands: Springer.

24. Debray F, Fautrelle Y. 1993 Electromagnetically driven parametric instability in an annular layer. In Chapter I: Dynamical systems and transition, in *Advances in Turbulence IV*, Applied Scientific Research (ed. FTM Nieuwstadt), vol. 51, pp. 31–36. Dordrecht, The Netherlands: Kluwer Academic. (doi:10.1007/BF01082510)

25. Ingwiller F, Bonnel F, Fautrelle Y, Daugan S, Etay J. 2001 Dynamique d'une goutte de métal liquide soumise à un champ magnétique alternatif. In *Proc. 9ème Colloque Francophone FLUVISU'2001, Rouen, France, June 2001*, pp. 129–134.

26. Fautrelle Y, Sneyd AD. 2005 Surface waves created by low-frequency magnetic fields. *Eur. J. Mech. B/Fluids* **24**, 91–112. (doi:10.1016/j.euromechflu.2004.05.005)

27. Burguete J, Miranda MA. 2012 Instabilities of conducting fluid layers in cylindrical cells under the external forcing of weak magnetic fields. *Magnetohydrodynamics* **48**, 69–75. See http://mhd.sal.lv/contents/2012/1/MG.48.1.9.R.html.

28. Foucault L. 1858 Description des procédés employés pour reconnaitre la configuration des surfaces optiques. *C. R. Acad. Sci.* **47**, 958–959.

29. Cerissier P, Jamond C, Pampaloni J. 1987 Wavelength selection in Bénard–Marangoni convection. *Phys. Rev. A* **34**, 1949–1952. (doi:10.1103/PhysRevA.35.1949)

30. Koshmider EL, Prahl SA. 1990 Surface-tension-driven Bénard convection in small containers. *J. Fluid. Mech.* **215**, 571–583. (doi:10.1017/S0022112090002762)

31. Manneville P. 1990 *Dissipative structures and weak turbulence*. Boston, MA: Academic Press.

32. Cortés-Domínguez I, Burguete J. Submitted. Instabilities of conducting fluid layers on weak time dependent magnetic fields. *Phys. Rev.*